A liquid MEMS inclinometer sensor with improved sensitivity

Xu, Han-yang; Zhao, Yu-long; Zhang, Kai; Wang, Zi-xi; Jiang, Kyle

DOI:
10.1016/j.sna.2018.11.046

Document Version
Peer reviewed version

Citation for published version (Harvard):
Xu, H, Zhao, Y, Zhang, K, Wang, Z & Jiang, K 2019, 'A liquid MEMS inclinometer sensor with improved sensitivity', *Sensors and Actuators A: Physical*, vol. 285, pp. 369-377. https://doi.org/10.1016/j.sna.2018.11.046

A liquid MEMS inclinometer sensor with improved sensitivity†

Han-yang Xu [1], Yu-long Zhao [1,*], Kai Zhang [1], Zi-xi Wang [2] and Kyle Jiang [3]

[1] State Key Laboratory for Manufacturing Systems Engineering, Xi'an Jiaotong University, Xi'an 710049, China; xuhanyang@stu.xjtu.edu.cn (X.-H.Y.); zhaoyulong@mail.xjtu.edu.cn (Y.-L.Z.); zhangkai1995@stu.xjtu.edu.cn (K.Z.)
[2] Xi'an Satellite Control Center, Xi'an 710043, China; Wongzx1023@163.com (W.-Z.X.)
[3] School of Mechanical Engineering, University of Birmingham, Birmingham B15 2TT, UK;k.jiang@bham.ac.uk;
* Correspondence: zhaoyulong@mail.xjtu.edu.cn; Tel.: +86-029-8339-5073

Abstract

This paper proposes a liquid microelectromechanical system (MEMS) inclinometer sensor and reports its design, fabrication, and characterization. In the sensor, a liquid metal droplet moves inside an annular-shaped channel, driven by gravity. The position of the liquid metal is reflected by electrodes and the new tilting angle is obtained. A MEMS fabrication process has been developed, and characterisation of the sensor has been carried out. Experiments show that the sensor has a resolution of 3.625° and a wide measuring range of ±45°. In comparison with solid MEMS gyroscopes, the proposed liquid sensor has advantages of fewer manufacturing steps and low costs. Beside, its resilience against impact is outstanding. Its sensitivity and accuracy are more than sufficient for hand held electronics, which are the main targeted applications of the proposed liquid sensor.

Keywords: liquid MEMS inclinometer sensor; sliding angle; super-hydrophobic; liquid metal droplet

1. Introduction

Microelectromechanical systems (MEMS) sensors have been developed and applied to a variety of civil and military fields, such as MEMS mechanical gyroscope [1, 2], quartz resonator [3], and micromachined inclinometer [4]. These sensors can measure accelerations, angles, displacements and positions in a moving system [5]. The vast majority of MEMS sensors are based on solid structures. In this area, beams, mass blocks and other solid structures have been widely used as sensing element. As sensing elements, solid structures offer high measurement accuracy and dynamic characteristics [6, 7]; however, due to the complexity of the related fabrication processes, the cost of these sensors is often high, and the ability to sustain overload is confined by the physical properties of the microstructures. Moreover, solid-solid contacts between mass block and frame are accompanied by strong friction, which may also lead to mechanical fatigue after long-term use.

The early metal liquid droplet applications for substituting the solid sensitive element can be traced back to the late 90s [8]. Most of the researches at the time focused on the selection of metal droplet micro-switches to provide on-off signals [9-11]. In further researches, liquid droplet was used as a sensitive element in various types of MEMS sensor, including the accelerometers [12], touch sensors [13], and gas sensors [14]. These kinds of liquid sensors have great advantages of high overload resilience, and the structure of the sensors is often simple that makes the fabrication process more convenient. However, research on liquid droplet inclinometer sensors is difficult to find. In 2010, Park reported a droplet digital accelerometer sensor based on MEMS technology (the sensor was used to measure the angle signal as well) [12]. The position of a metal droplet in the sensor changes with

acceleration and a number of electrodes are connected. Readings are taken from the electrodes to reflect the accelerations. The sensor could measure a range of acceleration signal from 0 to 40g. However, the resolution of the angle signal was not accurate (12°, 30°). In 2018, Cheng Li reported a liquid droplet tilt sensor based on optical fiber Fabry-Perot interferometric detection [15]. A liquid mercury droplet was used as the sensing element for tilting angles in a range of ±90°, and the measurement accuracy was less than 0.77°. However, the sensor requires complex optical equipment process in tests, including an optical circulator with a wavelength resolution of 0.02nm. This increases the size and costs of the sensor. Meanwhile, due to the measurement method of the sensor, the manufacturing process is limited and cannot be combined with the MEMS process.

A liquid MEMS inclinometer sensor is proposed in this paper that uses a metal liquid droplet and a micro-structured groove. The proposed liquid sensor avoids frictions between the solid-solid structures of the solid-state sensors, increases the range and resolution of measurement signals, and reduces the overall size and manufacture costs as well. The sensor mainly consists of a bottom substrate with a hydrophobic annular groove and array electrodes, a middle layer with a channel groove, and an upper layer of package process. The pattern and geometric sizes of the annular channel in middle layer was designed according to the relationship between input and output signals of the MEMS sensor. Further research has analyzed the movement condition of the droplet on the upper surface of the bottom substrate groove, and then designed the sizes of the groove. A MEMS fabrication process of the sensor was proposed to suit the design specifications of the sensor. The MEMS inclinometer sensor has a wide measuring range of ±45° and a fine resolution of 3.625°. The sensitivity of the sensor is improved by applying a highly hydrophobic layer in the microchannel. The research work contributes to the sensor research community in the following aspects: (1) proposed a liquid MEMS inclinometer sensor in which a liquid metal droplet is flowing inside a microchannel with treated surfaces; (2) The angle the liquid metal starts roll along a treated microchannel is measured and analyzed; and (3) the fabrication process of a liquid MEMS sensor is verified.

2. Device concept and design

2.1 Structure of the Sensor

Fig. 1 shows the schematic diagram of Liquid MEMS inclinometer sensor. The sensor consists of a bottom substrate (simplified to Sub-B), an upper layer (simplified to Lay-U), and a middle layer (simplified to Lay-M). A microscale liquid droplet was placed in the annular-shaped channel on the Lay-M, and the droplet provided angle signals when the input angle was changed. Here, the material properties of the metal droplets need to satisfy the following characteristics. First, the metal droplets must be able to conduct electricity; second, the metal droplets must have a large density; and third, the metal droplets must have a large surface tension. Therefore, a mercury droplet is used in the study. An annular groove was etched into the Sub-B. The groove has hydrophobic surfaces to reduce resistance for the metal to roll. Annular electrodes were deposited on the Sub-B by a sputtering process. The electrodes are arranged as such that the liquid droplet connects at least two adjacent electrodes. The tilting angle of the sensor shown as rotation direction of sensor in Fig.1 lets liquid droplet move and connect neighboring electrodes. The titling angle of the sensor can be reflected by the change of resistance between the connected electrodes. In addition, the Lay-U encapsulated the entire sensor structure, and a gap was left between the Lay-U and liquid droplet to ensure the same pressure at the both sides of the droplet.

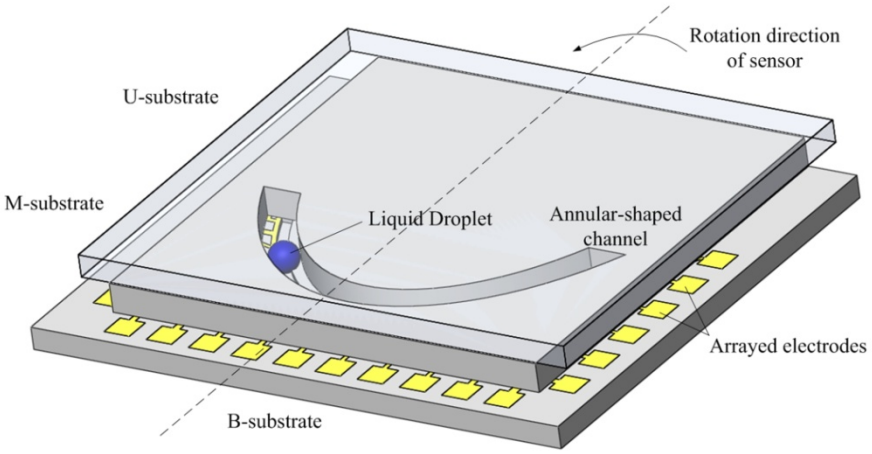

Figure 1. A schematic diagram of the liquid MEMS inclinometer sensor structure

2.2 Working Principle of the Sensor

The Liquid MEMS inclinometer sensor was developed based on the change of the droplet position in the annular channel, and the working principle is described as follows:

The sensor was placed in the vertical direction of the measured position, and angle between the sensor and the horizontal plane was α_0. Meanwhile, liquid metal droplet was placed at the lowest point in the annular-shaped channel on the Lay-M under the action of gravity and surface tension, and stayed on the groove of the Sub-B, as shown in Fig. 2. The movement tract of the droplet was dominated by annular channel in the Lay-M, and the groove on the Sub-B provided a hydrophobic surface for the liquid metal droplet. Besides, the stationary droplet contacted with the array metal electrodes on the surface of the Sub-B. Applied angle induced an inertial force on the droplet, which caused the movement and further changed the position of the droplet. Location of liquid metal droplet was conducted to sense by determining which two electrodes are connected. Furthermore, the final position of the droplet was used to calculate the output angle.

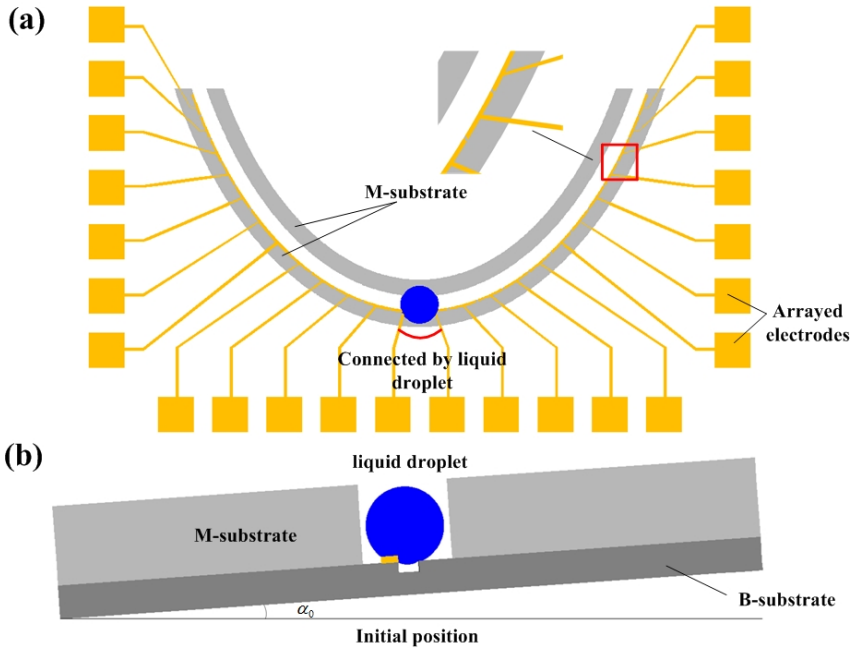

Figure 2. A schematic of the working principle of Liquid MEMS inclinometer sensor. (a) is the top view of the sensor in initial position, and (b) is the side view of the sensor.

2.3 Design Sturcture of the Channel on Lay-M

Liquid MEMS inclinometer sensor was placed at a specific angle with the horizontal surface during the measurement process, and trajectory of the liquid droplet was dominated by annular-shaped channel on the Lay-M. The pattern of channel here was designed to be elliptical, which satisfied the standard elliptic equation. In addition, the projection of the above elliptic curve in the vertical plane was also elliptical shape. To facilitate calculation, coordinate system 1 (X-Y-Z) and coordinate system 2 (X_1-Y_1-Z_1) were built in the inclined plane and vertical plane, as shown in Fig. 3(a) (Both of these two coordinates are changing with the rotation of the elliptical patterns). Fig. 3(b) shows the change of the elliptical patterns after the input angle α, and the rotation direction of the input angle is around the Z_0 (here, Z_0 is in the global coordinate of the total system, which does not change with the system rotation).The designed structure of the channel on Lay-M should satisfy the requirement that the input angle α equal to the sliding angle α_0 of droplet.

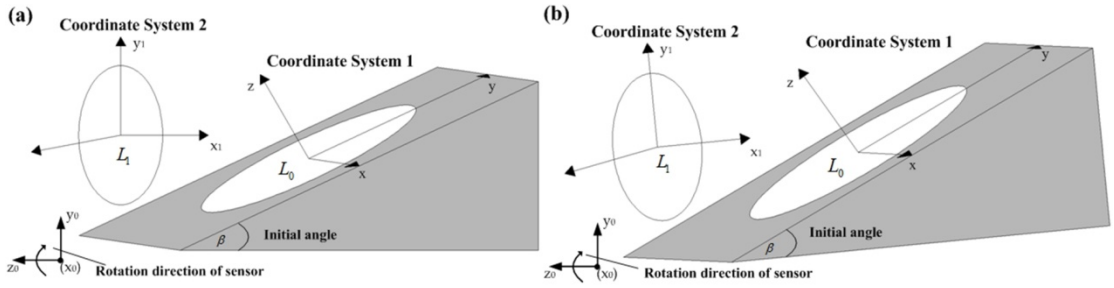

Figure 3. The pattern of grooves on Lay-M both in coordinate system 1 and coordinate system 2. (a) is the initial position of the structure, (b) is the structure position after input angle.

The channel on the Lay-M of the sensor in coordinate system 1 was satisfied with standard elliptic curve equation L_0.

$$\frac{x^2}{a_0^2}+\frac{y^2}{b_0^2}=1 \tag{1}$$

where, a_0 is the long axis radius of the elliptical curve in system 1, b_0 is the short axis radius, and x, y is the horizontal and vertical coordinates of the point on the elliptic equation of coordinate system 1.

The elliptic curve satisfied the elliptic curve equation L_1 in coordinate system 2.

$$\frac{x_1^2}{a_1^2}+\frac{y_1^2}{b_1^2}=1 \tag{2}$$

where, a_1 and b_1 is the radius of the long axis and the short axis of the projected elliptic curve in system 2 respectively, and x_1, y_1 is the horizontal and vertical coordinates of the point on the elliptic equation of coordinate system 2. In addition, $a_1=a_0$, $b_1=b_0\times\sin\beta$. B is the angle between the horizontal plane and the initial position of the sensor.

The liquid metal droplet was placed at the lowest point A of the ellipse-shaped channel by the combined action of gravity and surface tension. At the same time, the corresponding position of liquid droplet on projection elliptic curve L_1 was A_1, as shown in Fig. 4(a). The sensor was rotated around the Z_0-axis under the effect of input angle α, so that the liquid droplet overcame surface tension and started to slide in the channel. The metal droplet eventually stopped at the lowest point of the potential energy B(x_B, y_B) in coordinate system 1, and the projection point of B in the vertical plane was B_1(x_{B1}, y_{B1}), as shown

in Fig. 4(b). L_{b1} is the tangent line of point b_1 on curve L_1, and the slope of tangent line L_{b1} in the coordinate system is *tanα*.

$$\tan\alpha=\frac{x_{B_1}b_1^2}{y_{B_1}a_1^2} \tag{3}$$

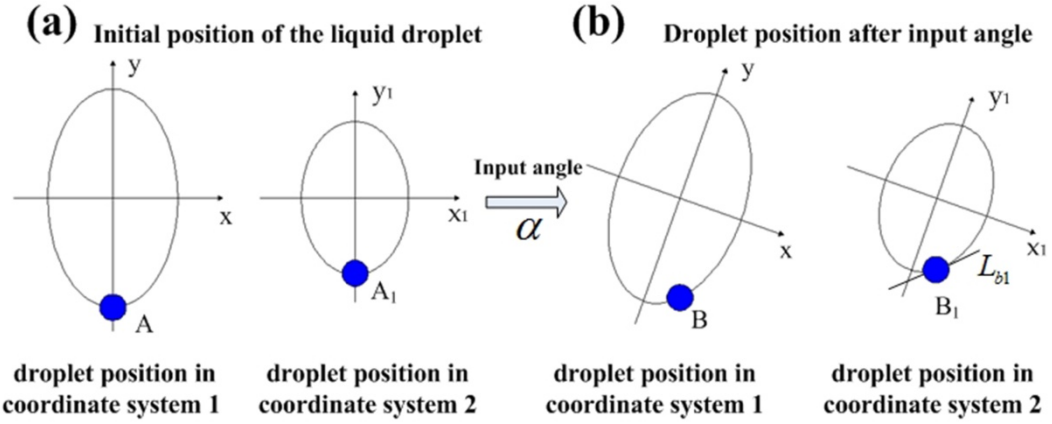

Figure 4. The liquid droplet position in groove on Lay-M. (a) is the initial position of the liquid droplet, (b) is the droplet position after input angle.

With the Combination of Eq. (1), (2) and (3), the angle at which liquid droplet slid in the elliptic curve channel on the Lay-M after sensor rotated by an input angle around the Z_0-axis was α_0, the relationship between *tanα* and $tan\alpha_0$ is shown as the following formula.

$$\tan\alpha=\frac{x_{B_1}b_1^2}{y_{B_1}a_1^2}=\frac{b_0^2}{a_0^2}\sin\beta\frac{x_B}{y_B}=\frac{b_0^2}{a_0^2}\sin\beta\tan\alpha_0 \tag{4}$$

In order to make the input angle α equaled to the sliding angle α_0 of the droplet in the annular-shaped channel, the following requirement must be met:

$$\frac{b_0^2}{a_0^2}\sin\beta=1 \tag{5}$$

As we can see, the structure sizes of annular-shaped channel on Lay-M mainly relate to long axis radius a_0, and short axis radius b_0, both of them are affected by the angle β between the initial position and the horizontal plane of the sensor.

2.3 Geometric Sizes of the Groove on Sub-B

The annular-shaped channel on the Lay-M provides a movement trajectory for the liquid droplet. Besides, the groove on the Sub-B provides a hydrophobic surface and facilitates easy movement of the droplet. As early as 1805, Thomas Young had already proposed the contact angle equation of flat surface [16]. Afterwards, with the complexity of the surface structure, current models with the microstructure surface are mainly based on Cassie-Baxter model and Wenzel model. The bottom of the droplet in Wenzel model is in contact with the entire micro-structure substrate [17], while droplet is only in contact with the surface of micro-structure substrate of the Cassie-Baxter model [18]. The stable state of the liquid droplet on these two infiltration states are usually determined by the roughness and the area fraction of the micro-structure substrate [19,20]. According to the principle of the lowest tension energy, droplet tends to obtain a stable condition and a small sliding angle in the state of

Cassie-Baxter when the surface is a hydrophobic surface or the roughness is sufficient [21].

In order to keep the droplet in the stable Cassie-Baxter state, the geometry sizes of the groove (the width of the groove *d* and the depth of the groove *h*) on the Sub-B need to be properly designed. The metal liquid droplet was placed on the groove of Sub-B and was in contact with the upper surface of the groove but without contacting the bottom surface of the groove as shown in Fig. 5 (a). Here, we consider that when the liquid is sliding slowly on the tilted surface, the rear contact line begins to move forward, which leads to the solid-liquid interface replaced by the gas-liquid interface, and then changes the surface energy of liquid [22]. Furthermore, the potential energy decreases with the droplet sliding downward. Ideally, the amount of the change in surface energy is equals to the change amount of potential energy. The sliding condition of liquid droplet on upper surface of groove is shown as Fig. 5(b), when the input inclination angles reach to α, the droplet stays in the critical sliding state (The rear contact line moves forward, and the front contact line is static), and the area of the rear contact line moves is ΔS, hence the amount change of the droplet surface energy ΔE can be:

$$\Delta E = (1+\cos\theta)\gamma_{lv}\Delta S \tag{6}$$

where γ_{lv} is the surface tension of mercury droplet, θ is the contact angle between droplet and groove upper surface, and ΔS is the approximate area of the solid-liquid interface being replaced by the gas-liquid interface, as shown in the red part of the Fig. 5(b). The amount value of the ΔS is:

$$\Delta S = \frac{\Delta x}{r}\left[r^2 \arccos\left(\frac{d}{2r}\right) - \frac{d}{2}\sqrt{r^2 - \left(\frac{d}{2}\right)^2}\right] \tag{7}$$

where *r* is the radius of the contact area between the droplet and the groove upper surface, *d* is the width of the groove, and Δx is the virtual displacement of the rear contact line moving forward.

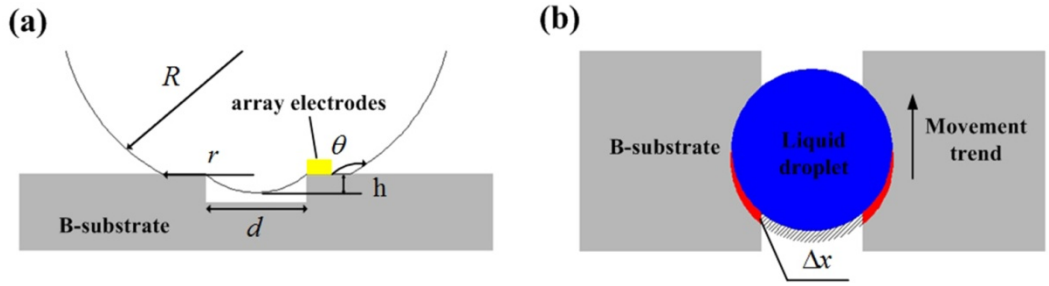

Figure 5. (a) Metal droplet sitting on the groove of Sub-B. (b) Droplet sliding on the groove, and the virtual displacement of the rear contact line is Δx

The liquid droplet slides down from the inclined surface when the sliding angle is α, and the downward movement amount of the barycenter is numerically equal to the of virtual displacement rear contact line Δx, then the change amount of the potential energy of liquid droplet $\Delta E'$ is:

$$\Delta E' = mg\Delta x \sin\alpha \tag{8}$$

where, *m* is the mass of droplet, *g* is the acceleration of gravity, α is the critical sliding angle. According to the conservation of energy, the relationship between sliding angle α and width of the groove *d* is:

$$\gamma_{lv}(1+\cos\theta)\Delta S = mg\Delta x \sin\alpha \tag{9.1}$$

$$\sin\alpha = \gamma_{lv}(1+\cos\theta)\left[r^2 \arccos\left(\frac{d}{2r}\right) - \frac{d}{2}\sqrt{r^2 - \left(\frac{d}{2}\right)^2}\right] \Big/ rmg \qquad (9.2)$$

Table 1 is the experimental data of the sliding angle and groove width of the mercury droplet on the silicon groove.

Table 1. The experimental data of the sliding angle

diameters of droplet (μm)	Width (μm)	Sliding angle
600μm	180	29.8°
	200	22.6°
	220	17.3°
	240	13.1°
	260	8.8°
	280	5.7°
	300	2.0°

Here, the contact angle of mercury droplet on silicon wafer with groove is 147°, and the surface tension of mercury is 0.485N/m. The experimental data were compared with the data obtained from the formula (9.2). Fig. 6 shows the relationship between the sliding angle α and the groove width d on the Sub-B. As can be seen from the figure, when the diameter of the droplet is definite, the sliding angle decreases with the increasing of the groove width. This is due to the increase of the groove width, which makes the lack of contact area between the droplet and the groove, and makes the droplet easier to separate from the surface. The blue line in figure 6 shows the experiment data of 600μm diameter of liquid droplet sliding on the various widths of silicon groove surface, the experimental results are in coincidence with theoretical results. In addition, Microscale liquid droplet is dislodged from the upper surface of groove and then fall into the bottom side of the groove when the width of the groove is large enough (the width is greater than 400μm). Besides, the array electrodes of the sensor were deposited on one side edge of the upper surface of groove in the Sub-B and as shown in Fig. 5(a), and the liquid droplet needs to be in contacted with the array electrodes at the time of sliding, so that the groove width d is not too large, d is 200±50μm in the design.

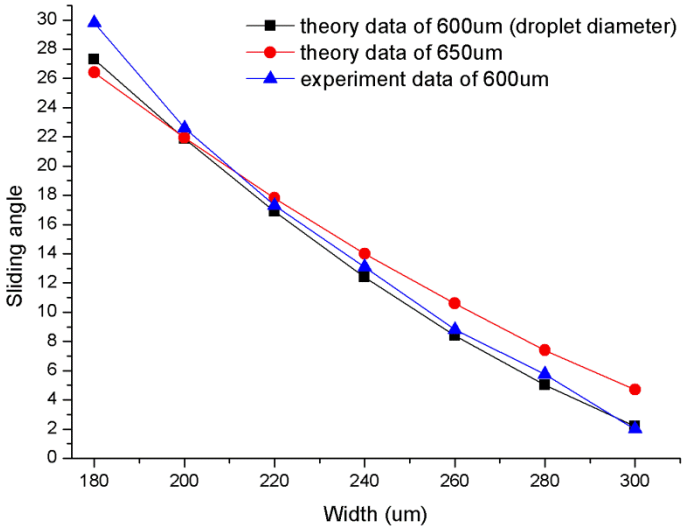

Figure 6. The relationship between the sliding angle and the width of the groove on the Sub-B

In order to maintain the stable Cassie-Baxter state of the liquid metal droplets, the depth of the groove on the Sub-B should be designed that the droplet does not contact with the bottom of the groove [23].

Based on the designed geometric sizes in Fig. 5(a), the formula for the minimum height h from the lowest point of the droplet (the lowest point of meniscus-shaped droplet on the groove) to the upper surface of the groove is shown as below:

$$h_{\min} = \frac{d}{2}\left(\frac{1-\sin\theta}{\cos(\pi-\theta)}\right) \tag{10}$$

where, d is the width of groove, and θ is the static contact angle of liquid droplet.

3. Fabrication process of typical sensor

Based on the theoretical analysis mentioned above, the manufacturing process of the liquid MEMS inclinometer sensor is designed, as shown in Fig. 7 (the prefabricated tilt angle of the sensor on the incline plane is 20°). The fabrication process consisted of the Sub-B, the Lay-M and the overall packaging process (the diameter of liquid droplet was 600μm in the process). For the Sub-B, the width of the groove was 200μm, and the depth was 100μm, the geometric pattern of the array electrode was shown as Fig. 2. The elliptical-shaped array electrodes were made up by 24 unconnected electrodes, and the ellipse curve accounted 1/4 for the whole ellipse perimeter, so that the array electrodes were able to measure about ± 45°. The distance between each electrode was about 20μm, which ensured that the liquid droplet was able to connect each two adjacent electrodes during the process of motion. Fig. 7 (a) shows the fabrication process for the Sub-B.

First, a layer of silicon dioxide with a thickness of 150nm was deposited on the surface of the monocrystalline silicon wafer by Plasma Enhanced Chemical Vapor Deposition (PECVD) process. After that a layer of photoresist (EPG 535) was sprayed on the silicon substrate which had covered with silica before, the photo mask was used in this step to expose the array pattern on substrate (the width of the array electrodes were about 40μm). Later, the Ni/Cr metal film (thickness of film was

approximately 150μm) was sputtered to the wafer substrate by radio frequency (RF) method using a magnetron sputtering machine. Second, a film of photoresist (AZ4620) was coated on the substrate, and then, the second photo mask was used in this step to expose the elliptical-shaped ring pattern (The patterns were close to the edge of the array electrodes, and the width of the ring was about 250μm.) Finally, the prepared substrate was etched by Inductively Coupled Plasma (ICP) machine, and the exposed ring pattern formed an annular groove (the depth of groove was about 100μm).

The position of the annular-shaped groove on the Lay-M was concentric with the groove on the Sub-B, and the geometric pattern was 1/4 ellipse (The long axis and short axis of the elliptic curve were 4.5mm and 7.5mm respectively).

The fabrication process of the Lay-M is shown as Fig. 7 (b). First, a 100μm SU-8 1070 photoresist was coated on the Sub-B surface to cover the etching annular groove. After that, a layer of 200μm SU-8 2150 photoresist was coated on the surface of the photoresist, and the above steps were repeated 3 times, the thickness of the photoresist was attained about 650μm. Second the third photo mask was used in this step to expose the ring channel pattern, the width of pattern was about 750μm, and the thickness was about 650μm. Finally, the ring channel pattern was removed by using the developer (the developer here was PGMEA), and the develop time was about 30min.

Fig. 7 (c) shows the overall packaging process of the liquid MEMS inclinometer sensor. The mercury droplet with radius of 300μm was injected into the annular-shaped channel on the Lay-M by micropipette. After that, UV-curable adhesive (Dymax 3016) was distributed in the Lay-U (the material of the Lay-U was Borosilicate glass, and the geometric size was *12.5×11.1mm*), and the 3 layers were bonded together.

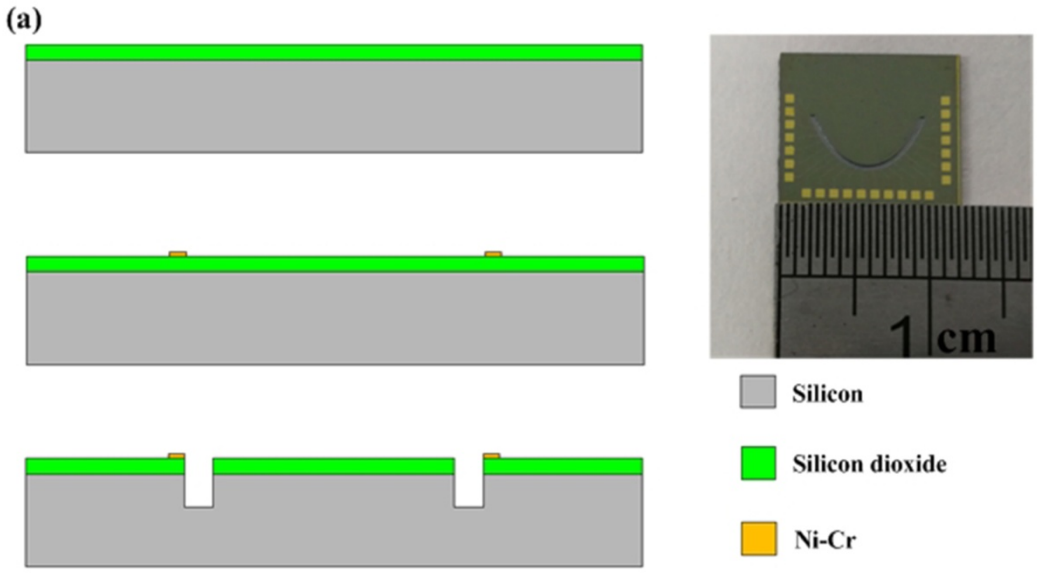

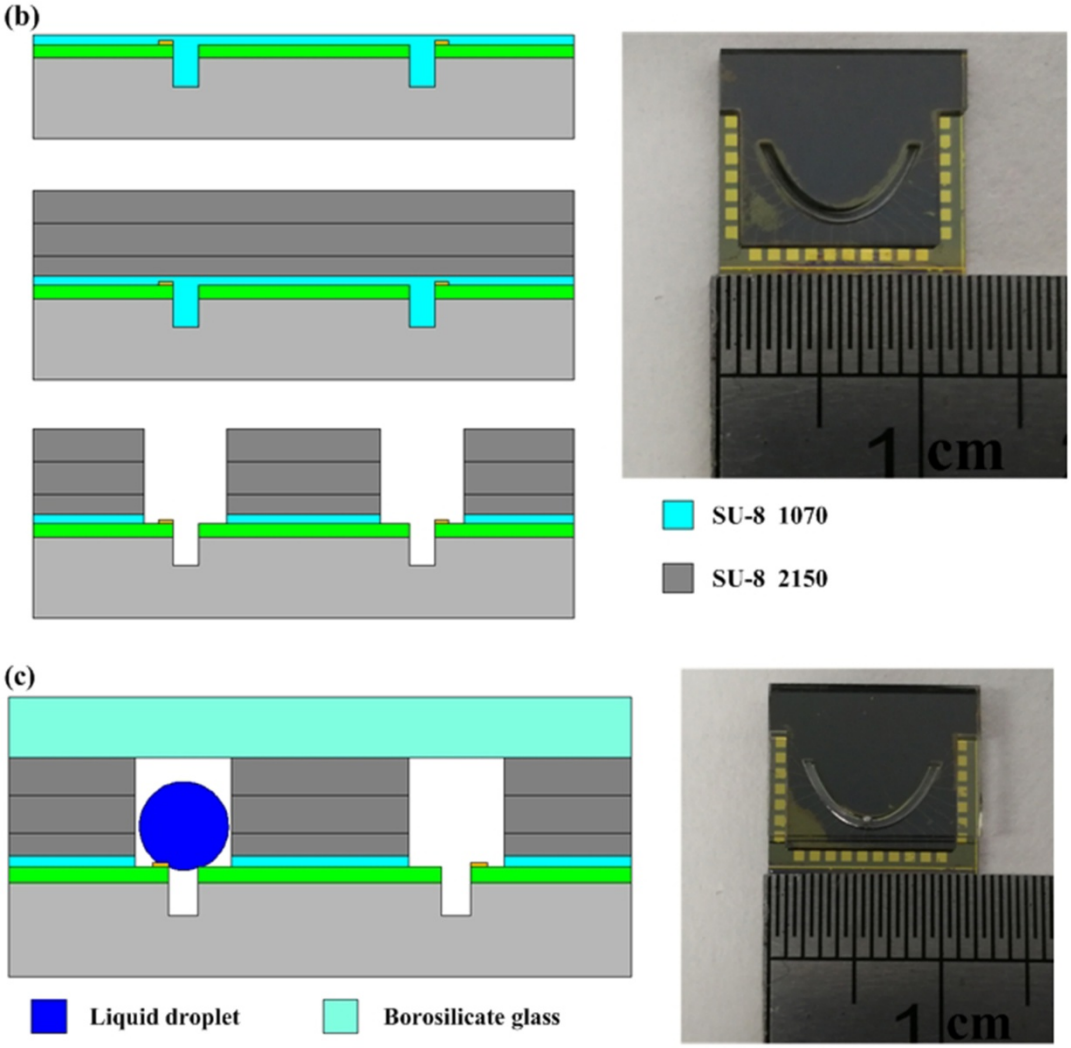

Figure 7. The schematic illustration of fabrication process. (a) is the fabrication process of Sub-B. (b) is the fabrication process of Lay-U. (c) is the overall packaging process of the liquid MEMS inclinometer sensor.

4. Results and Discussion

4.1 Effect of Oxygen Plasma Degumming Process on Contact Angle of the Droplet

The liquid metal droplet was placed in the annular-shaped channel on Lay-M with 2 types of model, as shown in Fig. 8. Fig. 8(a) shows the stable type, which means liquid droplet not connected with the sidewall of channel, in addition, Fig. 8(b) shows the state that droplet connected with sidewall. Without Hydrophobic treatment the connect angle of SU-8 photoresist and Lay-M is 148.5°, the effective Hydrophilic effect made the liquid metal droplet more like to be in type b, hence blocked the sliding of liquid metal droplet.

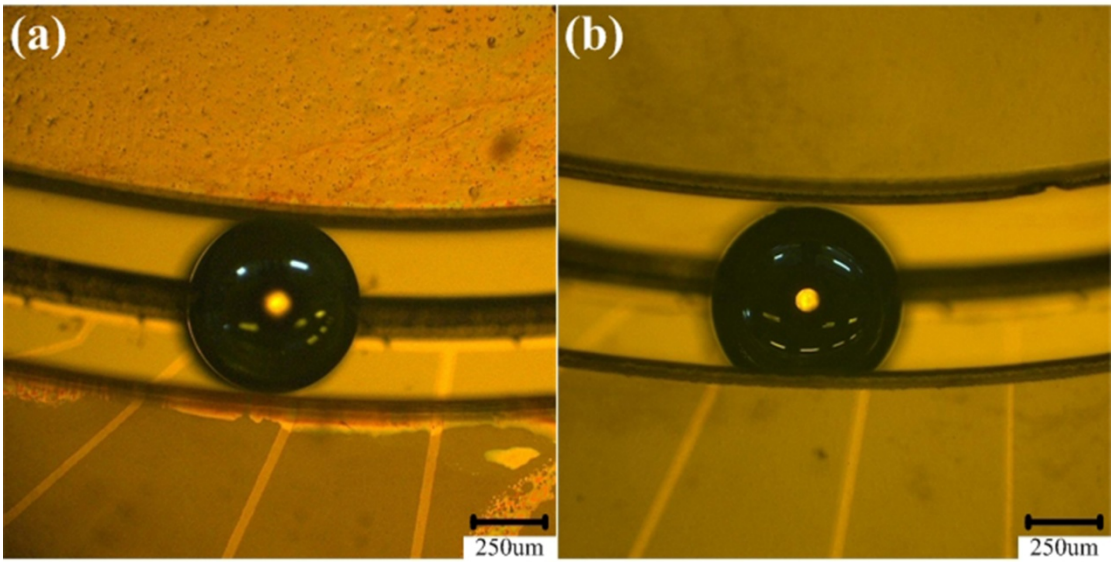

Figure 8. A liquid droplet is placed in the channel on Lay-M. (a) is the groove with 200W, and 2min treatment of oxygen plasma, (b) is the groove without hydrophobic treatment.

As mentioned above, liquid droplet obtain higher contact angle on rough surface, and tend to roll. The Sub-B and the Lay-M obtained in the fabrication process step B are treated by the oxygen plasma degumming process. The process provides a rough surface on SU-8 photoresist, table2 shows the data of processing parameters, surface roughness and contact angle after treatment by degumming machine.

Table 2. The data of processing parameters, surface roughness and contact angle

Power of plasma (W)	Treatment time (min)	Surface roughness(μm)	Contact angle
0	0	0.325	148.5°
100	1	0.632	152.5°
100	1.5	0.927	158.3°
100	2	1.135	159°
200	1	0.842	157°
200	1.5	1.289	161.5°
200	2	1.476	162°

With the increase of treatment time and plasma power, the roughness of SU-8 photoresist surface increases gradually, as well as the contact angle of liquid metal droplet on the photoresist surface. The surface of SU-8 photoresist appears property of superhydrophobic, and the liquid droplet on the surface tends to be stationary in the stable type mode. Meanwhile, the oxygen plasma treatment will form a self-limiting layer on the surface of the metal film [24,25]. This layer structure makes the surface energy of the metal rise, and causes the contact angle between the droplet and the metal surface increase, as shown in Fig. 9. (The material of the metal film is Cr and the thickness is 150nm).

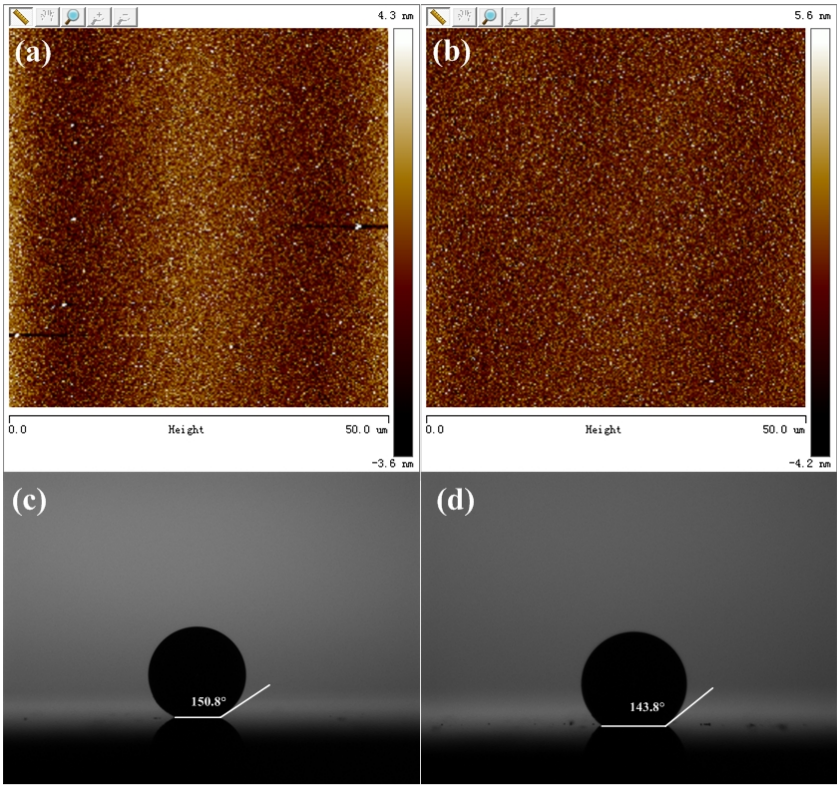

Figure 9. Effect of oxygen plasma treatment on the surface of Cr metal film. (a) is the surface without oxygen plasma treatment, (b) is surface with 200W plasma power and 2 min process time. The images are obtained by the Atomic Force Microscope (AFM), Bruker INNOVA. (c), (d) are the corresponding contact angle.

Table 3 shows the relationship between process parameters, surface roughness and contact angle after oxygen plasma treatment. The plasma degumming process has little effect on the roughness of the metal film surface. The process only provides nano-scale microstructure on the surface of the metal film, and the roughness of the metal surface is about 1 nm. In addition, with the increase of plasma power and treatment time, the contact angle between metal mercury droplets and Cr surface decreases gradually. This is due to the formation of a self-limiting layer on the surface of metal Cr film, which is more hydrophilic than the surface of metal Cr.

Table 3. The data of processing parameters, surface roughness and contact angle

Power of plasma (W)	Treatment time (min)	Surface roughness(μm)	Contact angle
0	0	0.884	150.8°
100	1	0.943	150.7°
100	1.5	0.865	150.1°
100	2	0.956	149.3°
200	1	0.922	146.5°
200	1.5	0.968	145.0°
200	2	1.198	143.8°

In the design and manufacture of the sensor, the groove on the Sub-B was mainly used to reduce the contact area between the metal droplet mercury and the lower surface, so as to reduce the sliding angle of the metal droplet on the Sub-B. Oxygen plasma treatment was mainly used to treat the channel on the Lay-M formed by SU-8 photoresist. In order to make sure that the metal droplet is stay in a stable state in the channel, and the power of the degumming machine is selected as 200W, and the

degumming time is 2min.

4.2 Experimental verification of minimum sliding angle of sensor

To verify the minimum sliding angle of the sensor under test condition, the experiment system was placed on a tilting experiment bench, which was composed of an optical dividing head (SHTH SJJF-1), an input angle display and a digital multimeter, as shown in Fig. 10. The optical dividing head provided changing angles both in horizontal direction and vertical direction.

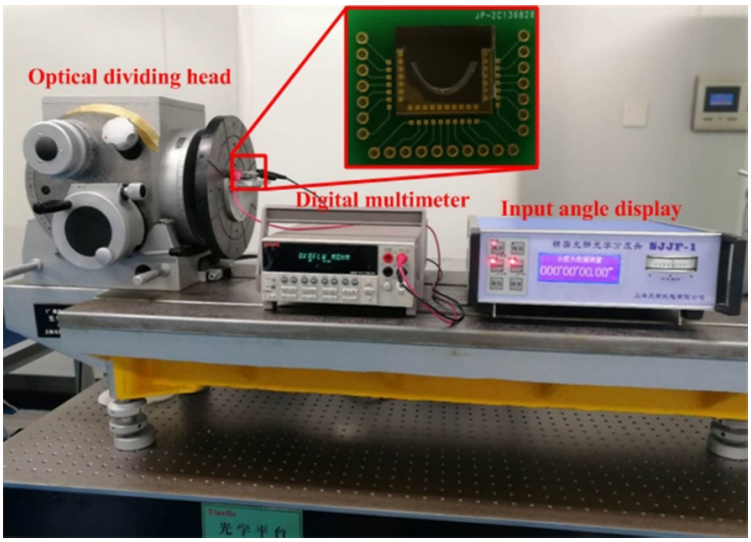

Figure 10. The bench for tilting experiments

The angle between initial position of sensor and the horizontal plane was β (20°), and liquid droplet was placed at the lowest point of the Lay-M as shown in Fig. 11(a). Two electrodes (number 1, 2) at the lowest point of the array electrodes were connected with each other through the liquid droplet, and the resistance value here was changed from infinity to the value shown in the digital multimeter, the value was about 3.0MΩ (The contact area of the mercury droplet and the array electrodes of the sensor was small. Furthermore, the force acted on the contact is only the gravity from the droplet, so the tinny contact area and the small force provided a large resistance on the contact surface. The resistance value here indicated that contact resistance was dominating). After that, the sensor rotated slowly around the Z_0-axis. When the sliding angle was 10.12°, the value of resistance on digital multimeter was changed into infinity again. In addition, microscopic showed that the location of the droplet was changed, as shown in Fig. 11(b).

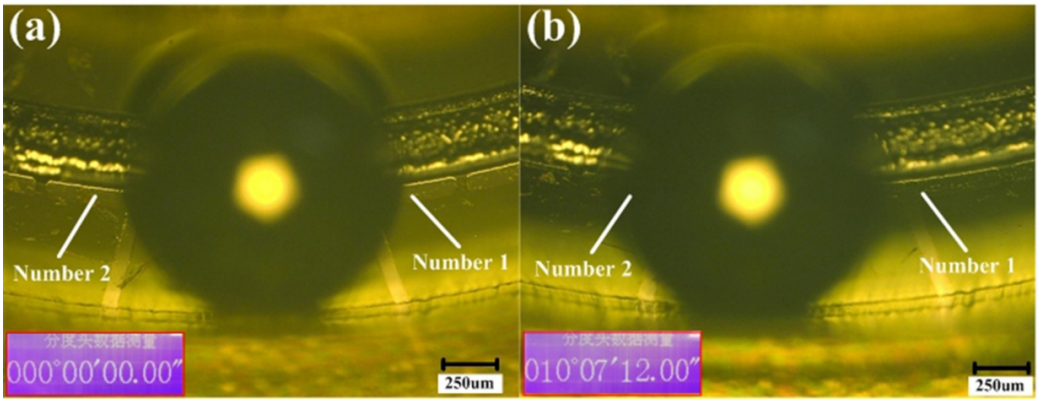

Figure 11. The sliding of the droplet in the sensor. (a) the position of droplet without input angle (the amount value of angle on display is 0°0'0", (b) the droplet position with input angle in 10.12° (10°7'12").

The experiment results show that the Liquid MEMS inclinometer sensor has a smaller initial sliding angle during measurement process, and the value of sliding angle is 10.12°. The contact angle between the liquid metal droplet and the Lay-M was 152°. The minimum sliding angle of the droplet was calculated as 8.8° using the formula (9.2), which had small error with the experimental validation. The main reason for this error is that the metal droplets connected with sidewall of the SU-8 photoresist on the Lay-M when sliding. The SU-8 photoresist treated by the oxygen plasma process will affect the minimum sliding angle of the metal droplets and cause the error of minimum sliding angle between experimental test and theoretical analysis.

As shown in Fig.6, the sliding angle of metal droplets decreases with the increase of the width of annular grooves on the Sub-B. The wider the width of annular grooves, the easier the metal slides. Meanwhile, the width of the annular groove ensures that the metal droplets do not fall into the groove. Therefore, the smaller minimum sliding angle can be obtained by increasing the width of the annular groove properly.

4.3 Experimental verification of resolution of sensor

The resolution of the sensor was mainly determined by the number of the array electrodes, the design number of array electrodes were 24 and the measurement interval was chosen to be ±45°, so that the resolution here was about 3.75°, In the experiment, the above experiment platform was used to test whether the sensor achieved the resolution of the design.

The 12 array electrodes in the same direction were connected one by one under the positive direction of clockwise rotation around Z_0-axis (the positive direction is defined as Z_0+), and the sensor was slowly rotated around the Z_0-axis. When the droplet was first contacted with two wires (such as 1, 2), the resistance value produced a signal and then continued to increase the input angle until the next pair of electrodes generated the indication. The rotated angle was the minimum resolution of the Liquid MEMS inclinometer sensor.

The results is showed as the following table, five array electrodes in the Z_0-axis+ direction were selected (number 5, 6, 7, 8, and 9).

Table 4. The rotation angle of different number of electrodes.

Number of electrodes	Rotation angle
5-6	3.2°
6-7	4.8°
7-8	3.1°
8-9	3.4°

It can be seen that when the droplet first connected the array electrodes and then moved to the next pair of electrodes, the rotation angle was 3.625°, which was close to the 3.75° of the design. At the same time, in order to obtain more accurate resolution, the number of array electrodes could be increased.

5. Conclusions

This paper proposes a liquid MEMS inclinometer sensor and provides details of the structure design, working principle and performance characteristics. The inclinometer sensor uses a microscale liquid droplet as the sensing element to avoid friction between solid structures. The sensor is constructed with three layers. An arc-shaped channel etched on Lay-M provides a curved channel for the droplet and the pattern was designed as 1/4 shape of ellipse with the long axis and short axis of the elliptic curve being 4.5 mm and 7.5 mm respectively. A groove was fabricated on the Sub-B to reduce

the sliding angle of the droplet and the geometry dimensions of the groove were design as 200±50um in width and 100um in depth.

The tilting experiments have verified the operational concept of inclinometer sensor. Liquid droplet started sliding in the channel under when the sensor was tilted and connected adjacent electrodes. The test results showed that the minimum sliding angle was 10.12°, which meaning the measurement range of designed sensor was ±10.12° to ±45°, and the resolution of the sensor was 3.625°. Furthermore, the number of electrodes and the width of annular grooves on M substrates can be increased to obtain more accurate resolution and larger measurement range. The research shows the simplicity of the liquid metal MEMS sensor, which has potential applications in hand-held electronics. The resilience of the sensor against impacts is a superior property, which enables the sensor to be used in extreme conditions where the solid MEMS sensors may not withstand.

Acknowledgments: The work was jointly by the Changjiang Scholars and Innovative Research Team in University of China (No. IRT_14R45), the National Science Fund for Distinguished Young Scholars (No. 51325503), and European Horizon 2020 project (No. 644971).

References

1. Sonmezoglu, Soner, Said Emre Alper, and Tayfun Akin. An automatically mode-matched MEMS gyroscope with wide and tunable bandwidth. Journal of microelectromechanical systems 23.2 (2014): 284-297.
2. Xie, Liqiang, et al. A z-axis quartz cross-fork micromachined gyroscope based on shear stress detection. Sensors 10.3 (2010): 1573-1588.
3. Uehara, Hiroshi, et al. Miniaturized angular rate sensor with laminated quartz tuning fork. Frequency Control Symposium and Exposition, 2005. Proceedings of the 2005 IEEE International. IEEE, 2005.
4. Billat, S., et al. Micromachined inclinometer with high sensitivity and very good stability. Sensors and Actuators A: Physical 97 (2002): 125-130.
5. Gaißer, A., et al. New digital readout electronics for capacitive sensors by the example of micro-machined gyroscopes. Sensors and Actuators A: Physical 97 (2002): 557-562.
6. Liu, Yan, et al. A high-performance multi-beam microaccelerometer for vibration monitoring in intelligent manufacturing equipment. Sensors and Actuators A: Physical 189 (2013): 8-16.
7. Zhao Y, Fang X, Jiang Z, et al. An ultra-high pressure sensor based on SOI piezoresistive material [J]. Journal of mechanical science and technology, 2010, 24(8): 1655-1660.
8. Simon, Jonathan, Scott Saffer, and C-J. Kim. A liquid-filled microrelay with a moving mercury microdrop. Journal of Microelectromechanical Systems 6.3 (1997): 208-216.
9. Kim, Joonwon, et al. A micromechanical switch with electrostatically driven liquid-metal droplet. Sensors and Actuators A: Physical 97 (2002): 672-679.
10. Shen, W., R. T. Edwards, and Chang-Jin Kim. Mercury droplet microswitch for re-configurable circuit interconnect. TRANSDUCERS, Solid-State Sensors, Actuators and Microsystems, 12th International Conference on, 2003. Vol. 1. IEEE, 2003.
11. Sen, Prosenjit, and Chang-Jin Kim. A fast liquid-metal droplet microswitch using EWOD-driven contact-line sliding. Journal of Microelectromechanical Systems 18.1 (2009): 174-185.
12. Park, Usung, Kwanghyun Yoo, and Joonwon Kim. Development of a MEMS digital accelerometer (MDA) using a microscale liquid metal droplet in a microstructured photosensitive glass channel. Sensors and Actuators A: Physical 159.1 (2010): 51-57.
13. Won, Dong-Joon, et al. Arrayed-type touch sensor using micro liquid metal droplets with large dynamic range and high sensitivity. Sensors and Actuators A: Physical 235 (2015): 151-157.
14. Shafiei, Mahnaz, et al. Utilizing p-type native oxide on liquid metal microdroplets for low temperature gas sensing. Materials & Design 122 (2017): 288-295.

15. Li, Cheng, et al. Room-Temperature Wide Measurement-Range Optical Fiber Fabry–Perot Tilt Sensor With Liquid Marble. IEEE Sensors Journal 18.1 (2018): 170-177.
16. Young, Thomas. III. An essay on the cohesion of fluids. Philosophical transactions of the royal society of London 95 (1805): 65-87.
17. Wenzel, Robert N. Resistance of solid surfaces to wetting by water. Industrial & Engineering Chemistry 28.8 (1936): 988-994.
18. Cassie, A. B. D., and S. Baxter. Wettability of porous surfaces. Transactions of the Faraday society 40 (1944): 546-551.
19. Lobaton, E. J., and T. R. Salamon. Computation of constant mean curvature surfaces: Application to the gas–liquid interface of a pressurized fluid on a superhydrophobic surface. Journal of colloid and interface science 314.1 (2007): 184-198.
20. Chen, Faze, et al. Hydrophilic patterning of superhydrophobic surfaces by atmospheric-pressure plasma jet. Micro & Nano Letters 10.2 (2015): 105-108.
21. Zheng, Q-S., Yang Yu, and Z-H. Zhao. Effects of hydraulic pressure on the stability and transition of wetting modes of superhydrophobic surfaces. Langmuir 21.26 (2005): 12207-12212.
22. Lv, Cunjing, et al. Sliding of water droplets on microstructured hydrophobic surfaces. Langmuir 26.11 (2010): 8704-8708.
23. Shen, Wenjiang, R. Timothy Edwards, and Chang-Jin Kim. Electrostatically actuated metal-droplet microswitches integrated on CMOS chip. Journal of microelectromechanical systems 15.4 (2006): 879-889.
24. Carey, Benjamin J., et al. Wafer-scale two-dimensional semiconductors from printed oxide skin of liquid metals. Nature communications 8 (2017): 14482.
25. Zavabeti, Ali, et al. A liquid metal reaction environment for the room-temperature synthesis of atomically thin metal oxides. Science 358.6361 (2017): 332-335.